bioRxiv preprint doi: https://doi.org/10.1101/2021.04.16.440130; this version posted April 16, 2021. The copyright holder for this preprint (which was not certified by peer review) is the author/funder, who has granted bioRxiv a license to display the preprint in perpetuity. It is made available under aCC-BY-NC-ND 4.0 International license.

1 # Oxford Nanopore and Bionano Genomics technologies evaluation for plant
2 # structural variation detection.

3

4 ## Authors:

5 Aurélie Canaguier[1], Romane Guilbaud[1], Erwan Denis[3], Ghislaine Magdelenat[3], Caroline
6 Belser[2], Benjamin Istace[2], Corinne Cruaud[3], Patrick Wincker[2], Marie-Christine Le Paslier[1],
7 Patricia Faivre-Rampant*[1] and Valérie Barbe[2]

8

9 ## Abstract

10 • **Background:**

11 Structural Variations (SVs) are very diverse genomic rearrangements. In the past, their
12 detection was restricted to cytological approaches, then to NGS read size and partitionned
13 assemblies. Due to the current capabilities of technologies such as long read sequencing and
14 optical mapping, larger SVs detection are becoming more and more accessible.

15 This study proposes a comparison in SVs detection and characterization from long-read
16 sequencing obtained with the MinION device developed by Oxford Nanopore Technologies
17 and from optical mapping produced by the Saphyr device commercialized by Bionano
18 Genomics. The genomes of the two *Arabidopsis thaliana* ecotypes Columbia-0 (Col-0) and
19 Landsberg *erecta* 1 (L*er*-1) were chosen to guide the use of one or the other technology.

20 • **Results:**

21 We described the SVs detected from the alignment of the best ONT assembly and DLE-1
22 optical maps of *A. thaliana* L*er*-1 on the public reference Col-0 TAIR10.1. After filtering, 1 184
23 and 591 L*er*-1 SVs were retained from ONT and BioNano technologies respectively. A total of
24 948 L*er*-1 ONT SVs (80.1%) corresponded to 563 Bionano SVs (95.3%) leading to 563
25 common locations in both technologies. The specific locations were scrutinized to assess

bioRxiv preprint doi: https://doi.org/10.1101/2021.04.16.440130; this version posted April 16, 2021. The copyright holder for this preprint (which was not certified by peer review) is the author/funder, who has granted bioRxiv a license to display the preprint in perpetuity. It is made available under aCC-BY-NC-ND 4.0 International license.

26 improvement in SV detection by either technology. The ONT SVs were mostly detected near
27 TE and gene features, and resistance genes seemed particularly impacted.
28 • **Conclusions:**
29 Structural variations linked to ONT sequencing error were removed and false positives limited,
30 with high quality Bionano SVs being conserved. When compared with the Col-0 TAIR10.1
31 reference, most of detected SVs were found in same locations. ONT assembly sequence leads
32 to more specific SVs than Bionano one, the later being more efficient to characterize large SVs.
33 Even if both technologies are obvious complementary approaches, ONT data appears to be
34 more adapted to large scale populations study, while Bionano performs better in improving
35 assembly and describing specificity of a genome compared to a reference.
36

37 **Keywords**

38 Structural variations, Oxford Nanopore technologies, Bionano Genomics Optical mapping,
39 High Molecular Weigth DNA, *Arabidopsis thaliana*.
40

41 Background

42 Structural variations (SV) are defined as genomic variations involving segments of DNA from
43 50 bp to several megabases. SVs consist of unbalanced rearrangements such as copy number
44 variations (CNV) including insertions/deletions (Indels) and presence/absence variations
45 (PAV), and balanced events like inversions and translocations [1,2,3,4]. Several mechanisms
46 explain the formation of SVs, such as recombination errors generated by non-homologous end-
47 joining and non-allelic homologous recombination, genome duplication and transposition [1,2].
48 The structural variations in human were largely studied and recently, Ho *et al*. reviewed the
49 impact of the SVs in human deseases [4]. In plants it has been shown that the structural
50 variations play a key role in evolution of genomes and are responsible for phenotypic variations

bioRxiv preprint doi: https://doi.org/10.1101/2021.04.16.440130; this version posted April 16, 2021. The copyright holder for this preprint (which was not certified by peer review) is the author/funder, who has granted bioRxiv a license to display the preprint in perpetuity. It is made available under aCC-BY-NC-ND 4.0 International license.

51 by impacting TEs and genes [3,5,6,7,8]. In particular, SVs were found in stress related and
52 resistance genes [9,10,11,12,13], to be related to local adaptation [14,15], or linked to other
53 traits of agronomical interest such as tomato fruit flavor, rice grain size or poplar wood
54 formation [16,17,18].
55 Nowaday, identification of SVs contributes to the construction of the Panreference genome or
56 super pangenome [19,20]. This new approach to build a reference will better reflect the genetic
57 diversity of the species, and in the same time deepen the understanding of genome evolution,
58 as well as enhancing knowledge of adaptative traits [21,22,23,24,25].
59 The development of new sequencing technologies has boosted studies of SVs found in a
60 genome, which were detected until recently only by CGH arrays or SNP [26,27,28]. Short read
61 sequencing technologies have made possible the identification of SVs in several species
62 [29,30,31,32,33,34,35,36]. However, the size of the reads is a limiting factor for the detection
63 of large SVs and SVs in highly repetitive regions. The 3rd generation sequencing offer new
64 opportunities to identify SVs at larger scale with two kinds of methods. First are based on linked
65 short reads, as in 10x Genomics and Hi-C approaches [37], second by directly generating long
66 reads, as proposed by Pacific Biosciences [38] and Oxford Nanopore Technologies (ONT)
67 [39,40]. These approaches provide access to complex regions, increasing their uses to produce
68 genome assemblies and to detect structural variations in human [4,41,42,43], in *Arabidopsis*
69 *thaliana* [24,44,45] and in other plants [46,47]. In parallel, a technology based on physical map
70 and developed by Bionano Genomics [48], generates information from very large DNA
71 molecules. These maps, named optical maps, are frequently generated to improve and validate
72 sequencing assembly, to detect SVs in human genomes [43,49,50,51,52] and more recently in
73 plants [7,46,47,53]. These 3rd generation sequencing data made possible the identification of
74 genetic rearrangements between individuals at intra specific level [53].

bioRxiv preprint doi: https://doi.org/10.1101/2021.04.16.440130; this version posted April 16, 2021. The copyright holder for this preprint (which was not certified by peer review) is the author/funder, who has granted bioRxiv a license to display the preprint in perpetuity. It is made available under aCC-BY-NC-ND 4.0 International license.

75 Herein, we obtained draft assemblies using Oxford Nanopore technology and Bionano
76 Genomics optical maps, in order to compare the detection and characterization of the structural
77 variations by both methods. Despite comparisons between two sequencing technologies or SV
78 detection softwares are not anymore an uncharted territory [24,43,44,54], the comparison of
79 two fundamentaly different technologies like ONT and Bionano was only performed in animals
80 (Chimpanze [52] and Drosophila [55]), but not yet in plants. *A. thaliana* is a model organism
81 with a small genome (130 Mb). For this study, we selected Columbia 0 (Col-0) and Landsberg
82 *erecta* 1 (L*er*-1), two of the most studied ecotypes.
83

84 Results

85 ONT sequencing and genome assembly

86 The ONT sequence data of *Arabidopsis thaliana* ecotypes, Columbia (Col-0) and Landsberg
87 *erecta* 1 (L*er*-1), were cleaned using the correction and trimming steps of Canu assembler [56].
88 A total of 9.8 Gb (N50=12.7 kb, 75X coverage) and 6.1 Gb (N50=16.5 kb, 47X coverage) were
89 obtained for Col-0 and L*er*-1, respectively (Additional file 1: Tables S1 and S2).
90 To estimate ONT data completeness, the cleaned Ler-1 ONT reads were aligned against the
91 L*er*-1 reference sequence with Minimap2 [57]. A total of 98.9% of the L*er*-1 reference sequence
92 was covered by ONT reads. These L*er*-1 ONT data were also mapped against the Col-0
93 TAIR10.1 genome that was 95.2% covered (Additional file 1: Table S3). Samtools *depth* tool
94 was then used on the L*er*-1 ONT reads mapping against the Col-0 TAIR10.1 reference to
95 estimate the coverage at each position. The average coverage of 100 kb windows was 46.9X,
96 with depth fluctuations in centromeric regions (Fig. 1).
97 To identify the best assembler for our data, *de novo* assemblies for Col-0 and L*er*-1 were
98 performed with Canu, RA and SMARTdenovo (SDN). Based on general statistics (assembly
99 size, contig number, N50 size), SMARTdenovo software generated better assemblies for both

bioRxiv preprint doi: https://doi.org/10.1101/2021.04.16.440130; this version posted April 16, 2021. The copyright holder for this preprint (which was not certified by peer review) is the author/funder, who has granted bioRxiv a license to display the preprint in perpetuity. It is made available under aCC-BY-NC-ND 4.0 International license.

100 ecotypes compared to Canu or RA. (Additional file 1: Tables S4 and S5). Indeed, the SDN
101 assemblies resulted in 79 contigs for Col-0 (cumulative size =117 Mb, N50=12.5 Mb with 5
102 contigs) and 101 contigs for L*er*-1 (cumulative sizes = 117 Mb, N50=10.7 Mb with 5 contigs).
103 In addition, chimeric contigs were observed with Canu, while assemblies were more
104 fragmented using RA (Additional file 2: Figures S1A-C and S2A-C). For all assemblers,
105 centromeric regions were covered by many small contigs. These results were also supported by
106 the alignements of the Col-0 and L*er*-1 assemblies on the respective reference chromosomes
107 Col-0 TAIR10.1 [58] and L*er* [44]. The SDN assemblies named ONT Evry.Col-0 and
108 Evry.L*er*-1 assemblies, were used to carry out subsequent SV analyses.

109 **Optical maps generation**

110 The labelling of the genomic DNA was carried out using staining protocol with DLE-1 enzyme
111 according to the manufacturer's protocol. One run per ecotype on the Saphyr device was
112 performed leading to 577.5 Gb and 610.9 Gb of molecules for Col-0 and L*er*-1 respectively.
113 Molecules larger than 150 kb were selected leading to about 600-fold final coverage based on
114 the theorical 130 Mb *Arabidopsis* genome size (Additional file 1: Tables S6 and S7). A total of
115 17 and 14 optical maps with N50 of 14.6 Mb and 14.7 Mb are generated for Col-0 and L*er*-1
116 respectively, bringing to a genome size of 125 Mb for both ecotypes (Additional file 1: Tables
117 S8 and S9).

118 The average label density of the L*er*-1 optical maps was estimated at 18.47 per 100 kb
119 (Additional file 1: Table S7). However, this DLE-1 density decreases in the centromeric regions
120 due to molecule depth diminution and optical map breaks (Additional file 2: Figures S3A-E,
121 Fig. 1).

122 **Structural Variations detection**

123 The detections of the structural variations were performed independently using the ONT and
124 Bionano technologies data and were carried out in two ways: L*er*-1 versus Col-0 TAIR10.1

bioRxiv preprint doi: https://doi.org/10.1101/2021.04.16.440130; this version posted April 16, 2021. The copyright holder for this preprint (which was not certified by peer review) is the author/funder, who has granted bioRxiv a license to display the preprint in perpetuity. It is made available under aCC-BY-NC-ND 4.0 International license.

125 reference and Col-0 versus L*er* reference. The different types of structural variations detected
126 in our study are described in Additional file 2: Figure S4. Because general SVs characteristics
127 (number, types and location) are similar in both types of analyses, only SV detection results
128 from the Evry.L*er*-1 assembly and optical maps against the Col-0 TAIR10.1 reference are
129 presented in details. Description of SVs detected by comparing the SDN assembly and optical
130 maps Col-0 with L*er* reference are provided in Additional file 1: Tables S10-S14 and Additional
131 file 2: Figures S5A-E.
132 The comparison of Evry.L*er*-1 assembly to Col-0 TAIR10.1 reference using MUMmer *show-*
133 *diff* utility [59] revealed 2 186 potential SVs (Table 1).
134
135 **Table 1.** Types of Evry.L*er*-1 ONT and Bionano SVs obtained after alignement against Col-0
136 TAIR10.1 reference.

SV Type	SEQ	BRK	JMP	TRA	INS/DEL/INV	TOTAL SV
ONT	108	6	5	NA	2 067	2 186
Bionano	NA	NA	NA	2	795	797

137 Note: NA : Not Available. SVs types are described in the Additional file 2: Figure S4.
138
139 A total of 119 SVs, called reference sequence junction (SEQ), break (BRK) and jump (JMP),
140 found in centromeric, telomeric and nearby rDNA cluster were considered to correspond to
141 unresolved assembly regions into Evry.L*er*-1 assembly compared to Col-0 TAIR10.1 reference
142 and were filtered out.
143 To avoid false positive SV detection due to the ONT high error sequencing rate of 7.5% [60],
144 a filter on query ONT structural variations size (> 1 kb) was applied. Out of the 2 186 SVs
145 initially detected, 1 184 SVs remained (54.2% of total SVs) corresponding to 591 insertions
146 (INS), 581 deletions (DEL) and 12 inversions (INV). No duplication was detected (Table 2).
147
148

bioRxiv preprint doi: https://doi.org/10.1101/2021.04.16.440130; this version posted April 16, 2021. The copyright holder for this preprint (which was not certified by peer review) is the author/funder, who has granted bioRxiv a license to display the preprint in perpetuity. It is made available under aCC-BY-NC-ND 4.0 International license.

149 **Table 2**. Characteristics of Evry.L*er*-1 ONT and Bionano SVs, obtained after alignement

150 against Col-0 TAIR10.1 reference.

Technology	**ONT**				**Bionano**				
SV type	**INS**	**DEL**	**INV**	**TOTAL**	**INS**	**DEL**	**INV**	**TRA**	**TOTAL**
SV > 1kb (%)	591 (49.9)	581 (49.1)	12 (1.0)	1 184	289 (48.9)	295 (49.9)	5 (0.8)	2 (0.4)	591
Cumulated Size	3.4	4.0	0.3	7.7	2.9	2.3	1.6	0.4	7.2
Median Size	3 358	3 446	17 012	3 455	4 383	4 296	166 007	189 454	4 383
Average Size	5 724	6 801	26 865	6 467	10 021	7 885	310 470	189 454	12 104

151 Note : Cumulated sizes are in Mb, Median and average sizes in bp.

152

153 A 5 Mb insertion in the Evry.L*er*-1 assembly was detected on Chr3 Col-0 TAIR10.1 reference
154 (14 272 986..14 284 724) due to a detection error of MUMmer in a complex region associated
155 to a rDNA cluster. Thereby, this insertion was removed from the final data and not considered
156 in the result. The ONT structural variations median size was 3 455 bp and the cumulated sizes
157 7.7 Mb. The SVs were equally distributed in size and number between INS and DEL. The INV
158 categories had larger median and average sizes than INS and DEL. With a cumulated size of
159 0.3 Mb, INV represented 3.9% of the ONT variation size (Table 2). Structural variations were
160 detected on all chromosomes, with a preferential location on chromosome arms and with no
161 confident SV on the Chr1, 3 and 4 centromeres (Fig. 1).

162 Bionano data analysis (optical maps construction and SVs detection) was carried out on the
163 Bionano Solve interface. Structural variations were highlighted by comparing optical maps
164 results to *in silico* Col-0 TAIR10.1 reference genome labelling with DLE-1. A total of 797 SVs
165 were identified during the analysis of L*er*-1 optical maps *versus* Col-0 TAIR10.1 reference
166 (Table 1). When Bionano Solve tools detected one SV embedded in a second one, the largest
167 SV was kept. This case was found on two Chr1 independent locations
168 (INS:19 432 310..19 468 513 and DEL:24 688 666..24 736 849). A 1 kb size filter was applied
169 on the Bionano SVs, that was equivalent to remove deletions and insertions with a Bionano

bioRxiv preprint doi: https://doi.org/10.1101/2021.04.16.440130; this version posted April 16, 2021. The copyright holder for this preprint (which was not certified by peer review) is the author/funder, who has granted bioRxiv a license to display the preprint in perpetuity. It is made available under aCC-BY-NC-ND 4.0 International license.

170 quality score < 10 (defined as poor quality by the manufacturer) (Additional file 1: Table S15).
171 Additionally, on Chr2, the INV SV (3 433 371..3 490 731) with no quality score was discarded.
172 Thereby, 591 SVs representing 74.2% of total Bionano SVs were further considered in this
173 analysis. INS and DEL types constituted the main part of the Bionano SVs (48.9% and 49.9%
174 of the SVs respectively), the remaining 1.2% corresponding to translocations (TRA) and INV
175 (Table 2). Median SVs size was 4 383 bp and SVs cumulated sizes represented 7.2 Mb of the
176 genome. The TRA and INV types corresponded to nearly one third (2.0 Mb) of the structural
177 variations cumulated size. In our study, the translocations were only detected using the Bionano
178 assembly. The two L*er*-1 TRA were located on Chr2 (3 378 844..3 397 121;
179 3 484 209..3 844 839) (Additional file 2: Figure S6). The largest SV identified was a 1.1 Mb
180 L*er*-1 INV located on Col-0 TAIR10.1 reference Chr4 (1 435 832..2 593 360) (Additional file
181 2: Figure S7). SVs were distributed preferentially along the chromosome arms and their
182 detection was limited in centromeric regions due to decreased in labelling in these regions (Fig.
183 1).

184 **SVs comparison**

185 SVs comparison was based on their absolute start- and end-positions on the Col-0 TAIR10.1
186 reference sequence. We considered structural variations were comparable in both technologies
187 when their locations overlapped by at least 1 bp. To go further, SVs identified by ONT and
188 Bionano technologies were assigned a two letters svID code with the first letter used for ONT
189 SVs, the second for Bionano SVs, leading to common (svID UU and MU) and specific (svID
190 UN and NU) locations (with “U” for “Unique SV”, “M” for “Multiple SVs” and “N” for “None
191 SV”, Additional file 1: Tables S16 and S17).

192 SVs comparison metrics are presented in Table 3. A total of 563 common locations were
193 identified representing 948 (80.1%) of ONT SVs and 563 (95.3%) of Bionano SVs. The
194 cumulated sizes of these common SVs are 5.9 Mb and 6.9 Mb for ONT and Bionano detection

bioRxiv preprint doi: https://doi.org/10.1101/2021.04.16.440130; this version posted April 16, 2021. The copyright holder for this preprint (which was not certified by peer review) is the author/funder, who has granted bioRxiv a license to display the preprint in perpetuity. It is made available under aCC-BY-NC-ND 4.0 International license.

195 respectively. ONT SVs tend to be smaller than Bionano SVs (Table 3, Additionnal File 1 Tables
196 S16 and S17).
197
198 **Table 3**. Characteristics of Evry.L*er*-1 ONT and Bionano SVs identified in common and
199 specific Col-0 TAIR10.1 locations.

Technology	ONT		Bionano	
	Common	**Specific**	**Common**	**Specific**
Locations	563	236	563	28
SVs > 1 kb (%)	948 (80.1)	236 (19.9)	563 (95.3)	28 (4.7)
Min Size	1 003	1 003	1 034	1 017
Max Size	87 533	347 239	1 143 224	166 007
Cumulated Size	5.9	1.8	6.9	0.3
Median Size	3 759	2 656	4 456	1 374
Average Size	6 221	7 453	12 171	11 104

200 Note : Cumulated sizes are in Mb, and all other sizes in bp.
201
202 Among the 563 common regions, 410 (72.8% of the common regions) coincided with svID UU,
203 *i.e.* one ONT structural variation corresponding to one SV Bionano. In most cases, the overlap
204 of these SVs was at least 50.0% of the ONT SV size, and 405 (98.8% of the svID UU) SVs
205 have conforming type (*i.e.* have the same type) (Additional file 1: Table S16). The remaining
206 five svID UU (1.2%) were identified as deletions by ONT and insertions by Bionano
207 technologies (svID UU_035, UU_038, UU_057, UU_073, UU_358; Additional file 1: Tables
208 S16 and S17).
209 In the remaining 153 (27.2%) common locations, a total of 531 of the ONT SVs (56.8% of
210 commons ONT SVs) related to the Bionano SVs (27.0% of commons Bionano SVs) were
211 pinpointed (Table 4). These structural variations had a svID MU. The cumulative size of this
212 SVs category is approximately 4 Mb for both technologies although the number of ONT
213 variants is 3.5 times higher than in Bionano (531 vs 153). Nevertheless, Bionano median and
214 average sizes are 2 and 4 fold larger respectively.

bioRxiv preprint doi: https://doi.org/10.1101/2021.04.16.440130; this version posted April 16, 2021. The copyright holder for this preprint (which was not certified by peer review) is the author/funder, who has granted bioRxiv a license to display the preprint in perpetuity. It is made available under aCC-BY-NC-ND 4.0 International license.

215 **Table 4**. Characteristics of the svID MU identified in ONT and Bionano SVs.

Technology	ONT	Bionano
Location	153	153
Number	531	153
Min Size	1 010	1 253
Max Size	87 533	1 143 224
Cumulated Size	3.9	4.4
Median Size	4 236	9 523
Average Size	7 406	28 734

216 Note: svID MU corresponds to locations where Multiple ONT SVs overlap a Unique Bionano
217 SV. Cumulated sizes are in Mb, and all other sizes in bp.
218

219 The largest ONT SV was a complex SV (svID MU_102; MU meaning that several ONT SVs
220 match to one Bionano SV) consisting of four contiguous deletions located on Chr4. These four
221 deletions coincided with one Bionano deletion (Additionnal file 1: Tables S16 and S17). The
222 largest Bionano SVs (svID MU_097) was an inversion on Chr4 of 1 143 224 Mb overlapping
223 22 SV ONTs (corresponding to INS and DEL) (Additionnal file: 1 Table S17).
224 Specific locations were more abundant with the ONT technology (236 SVs - 19.9%) than with
225 Bionano (28 SVs - 4.7%) leading to a cumulated size of 1.8 Mb and 0.3 Mb respectively, and
226 with a median size twice larger (2 656 bp for ONT SVs *vs* 1 374 bp for Bionano SVs). The
227 distribution of the specific ONT SVs onto the Col-0 TAIR10.1 chromosomes lead to a clear
228 trend to locate on NOR and centromeres (Fig. 1). The largest specific ONT variant is located
229 on Chr3 and corresponds to a DEL (svID UN_124; SV detected with ONT only, Additional file
230 1: Table S16). The largest specific Bionano SV is spotted on the Chr3 and corresponds to an
231 INV type (svID NU_017; SV detected with Bionano only, Additional file 1: Table S17). A
232 focus on the TRA revealed a 18.2 kb specific L*er*-1 Bionano SV (svID NU_007), close to the
233 second TRA of 360 kb positioned around 3.6 Mb (MU_153). This TRA coincided with seven
234 SV events (1 INV, 5 INS and 1 DEL) in the L*er*-1 SDN assembly (Additional file 1: Tables
235 S16 and S17).

bioRxiv preprint doi: https://doi.org/10.1101/2021.04.16.440130; this version posted April 16, 2021. The copyright holder for this preprint (which was not certified by peer review) is the author/funder, who has granted bioRxiv a license to display the preprint in perpetuity. It is made available under aCC-BY-NC-ND 4.0 International license.

236 Using Araport11 annotation of the Col-0 reference (The Arabidopsis Information Resource -
237 TAIR), a comparison using only ONT SVs is shown in Table 5. Since the Bionano events
238 represent a large-scale observation, they were not taken into account in this analysis. A total of
239 893 (75.4%) out of 1184 ONT SVs overlaped TE features, of which 579 also overlaped genes.
240 Only 291 (24.6%) SVs are located outside a TE feature, overlapping genes [125 (10.6%)] or
241 not [166 (14.0%)] (Table 5). Focusing on ONT specific SVs (svID=UN), their overlap with the
242 Col-0 reference annotation showed similar percentage compared to the common SVs.
243

244 **Table 5**. L*er*-1 ONT SVs (>1kb) overlapping Col-0 TAIR10.1 genes and TEs annotation
245 features.

Features		noTE		TE		TOTAL (%)
		noGENE	GENE	noGENE	GENE	
Common SV	UU	79	59	93	179	410 (34.6)
	MU	59	38	150	291	538 (45.5)
Specific SV	UN	28	28	71	109	236 (19.9)
SV number (%)		166 (14.0)	125 (10.6)	314 (26.5)	579 (48.9)	1 184
TOTAL (%)		291 (24.6)		893 (75.4)		1 184

246

247 To better characterize the genes affected by ONT SVs in common locations, a GO-terms
248 overrepresentation test was performed with the PANTHER's tool [61] available on TAIR
249 website (https://www.arabidopsis.org/tools/go_term_enrichment.jsp). Among the 1 764 genes
250 identified in common locations, 47.2% (832) genes were uniquely assigned to a GO term and
251 used in PANTHER (Additional file 1: Tables S18 and S19). Overrepresentations in defense
252 response and ADP-binding terms were detected (Additional file 1: Table S20), but no
253 enrichment for GO-terms in genes in specific ONT locations was highlighted (Additional file
254 1: Tables S21-S23).
255
256

bioRxiv preprint doi: https://doi.org/10.1101/2021.04.16.440130; this version posted April 16, 2021. The copyright holder for this preprint (which was not certified by peer review) is the author/funder, who has granted bioRxiv a license to display the preprint in perpetuity. It is made available under aCC-BY-NC-ND 4.0 International license.

257 # Discussion

258 Herein, we compare the performance of Oxford Nanopore and Bionano Genomics technologies
259 for structural variation detection. For this, we performed long read sequencing and optical
260 mapping of two *A. thaliana* ecotypes, namely Columbia-0 (Col-0) and Landsberg *erecta* 1
261 (L*er*-1). Long read *de novo* assemblies were constructed using three different assemblers and
262 optical maps were assembled with Bionano Solve tools. Structural variations detected using the
263 Col-0 TAIR10.1 [58] and L*er* [44] genomic sequences as references, were described and
264 compared to each other, to reveal the relative strengths of the two technologies in highlighting
265 SVs.

266 **Assemblies based on ONT and Bionano data for SV analyses**

267 To obtain the best assembly based on only long reads data we used three different assemblers.
268 After comparison of assembly metrics, calculation time and collinearity against reference
269 genomes, SDN provided the best assembly even if some collinearity breaks were observed,
270 especially in centromeric regions. The metrics of Evry.Col-0 and Evry.L*er* 1 SDN assemblies
271 were comparable to such assemblies in previous studies [24,44,45,62].

272 Continuous improvement in protocols and new developments in genome assembly strategies
273 and algorithms resulted in higher and higher quality of genomic sequences used in subsequent
274 analyses. Previously published Bionano *A. thaliana* optical map (KBS-Mac-74) genome [45]
275 used a BspQI staining protocol for labelling, generating about 10 time more maps to cover the
276 entire genome of KBS-Mac-74 than in our study (DLE-1 Bionano staining protocol),
277 highlighting enhancement in Bionano's protocol. In addition, no optical map was previously
278 available for the Columbia (Col-0) and Landsberg *erecta* 1 (L*er*-1), making our map assemblies
279 especially valuable for further studies.

280 Our high quality map allowed us to define centromeric and nucleolar organizer regions (NOR),
281 despite lower molecules density and even if label concordance loss were observed between L*er*-

bioRxiv preprint doi: https://doi.org/10.1101/2021.04.16.440130; this version posted April 16, 2021. The copyright holder for this preprint (which was not certified by peer review) is the author/funder, who has granted bioRxiv a license to display the preprint in perpetuity. It is made available under aCC-BY-NC-ND 4.0 International license.

282 1 maps compared to the Col-0 TAIR10.1 *in silico* reference maps. Moreover, fluctuations in
283 ONT coverage density and accumulation of repetitive alignments in the same regions are
284 reinforcing evidences of the approximate locations of the centromeres and NOR. However, we
285 identified several missassemblies in the course of our SVs analyses between the ONT SDN
286 L*er*-1 assembly and Col-0 TAIR10.1 reference, highlighting how difficult it can be to get a
287 reliable assembly, and thus detecting SVs, in these complex regions.

288 **SV detection and comparison between the two technologies**

289 Herein, we compared structural variations in Evry.L*er*-1 and the reference genome Col-0
290 TAIR10.1. We chose this reference because of its high quality and the richness of the associated
291 studies [24,44,45].

292 The cumulated SVs sizes obtained for ONT and Bionano in our study are smaller than in
293 previous studies [24,44]. Filtering on SVs size (SVs > 1kb *vs* no size filter) could explain this
294 difference. In addition, the lack of duplications detection in ONT assembly could depend on
295 MUMmer's ability to detect this type of SV, reflecting the detection complexity of the
296 duplication events, as mentioned in Goel *et al* (2019). In contrast, the absence of duplication
297 detected by Bionano could be explained by polymorphic duplications between L*er*-1 maps and
298 Col-0 TAIR10.1 reference, which would break the collinearity, as described in Jiao *et al.*
299 (2020), and by the size of duplications (< 5kb, [62]) identified as the limit of Bionano detection.
300 Analyzes by the two technologies revealed a predominance of insertion, deletion and inversion
301 with larger median and average sizes for Bionano SVs. The distribution of these types of SV is
302 homogeneous along the chromosomes arms. Even if most of the specific ONT SVs are located
303 in the centromeric and pericentromeric regions, a decrease coverage of the SVs in these regions
304 is probably due to technical problems such as assembly errors (for ONT SMARTdenovo). This
305 diminution in SV coverage is also observed with Bionano technology, showing a lower density
306 labeling in these complex regions. This contrasts with previous results identifying more SVs in

bioRxiv preprint doi: https://doi.org/10.1101/2021.04.16.440130; this version posted April 16, 2021. The copyright holder for this preprint (which was not certified by peer review) is the author/funder, who has granted bioRxiv a license to display the preprint in perpetuity. It is made available under aCC-BY-NC-ND 4.0 International license.

307 regions where the recombination meiotic rate decreases [24]. The filtering of SV ONTs smaller
308 than 1 kb could again be an explanation for this contradiction. On the other hand, Bionano Solve
309 tools well identified translocation previously characterized on Chr2 and three inversions larger
310 than 50 kb present on Chr3, Chr4 and Chr5 [24,35,44]. For example, compared to the Col-0
311 TAIR10.1 reference, the L*er*-1 maps support a 360 kb translocation of mitochondrial sequence
312 in the Chr2 around the 3.6 Mb Col-0 TAIR10.1 position (svID MU_153). This observation is
313 concordant with Stupar *et al.* (2001) that first described the mtDNA insertion in the Col-0
314 reference. In this Chr2 region (3.29 Mbp to 3.48 Mbp), Pucker *et al.* (2019) identified a second
315 300 kb highly divergent region between *A. thaliana* Nd-1 and Col-0 reference. In the same
316 study, Pucker *et al.* also described the lack of the entire region between 3.29 Mbp and 3.48 Mbp
317 in L*er* genome, corresponding to the specific translocation of 18.2 kb detected in L*er*-1 map
318 (svID NU_007). Zooming in this Col-0 TAIR10.1 Chr2 region (3.2 Mb to 3.5 Mb) in the
319 L*er*-1 SDN assembly, many small contigs are observed with a missing sequence of 110 kb. This
320 observation explains absence of SV detection, confirming the great complexity of this region
321 and the sequence divergence between L*er*-1 and Col-0 genome described by Pucker *et al*
322 (2019). Even if the Col-0 reference sequence has been improved since 2000 [58], our assembly
323 (Evry.Col-0) confirms its value to re-evaluate complex region assembly, and provide new high
324 quality optical map data.

325 The number, type and location of SVs in the largest common ONT (svID MU_102) and
326 Bionano (svID MU_097) SVs, as well as the Chr2 ONT SVs matching the second Bionano
327 translocation (svID MU_153), reflect that the structural variations brought out by ONT were
328 more numerous and smaller, which allows an identification at finer scale. In contrast, Bionano
329 variants were larger and their sizes depend on restriction sites distribution.

330 To globally estimate consistency of the SV analyzes between ONT SDN or Bionano L*er*-1
331 assemblies against Col-0 TAIR10.1 reference, we compared the structural variations we

bioRxiv preprint doi: https://doi.org/10.1101/2021.04.16.440130; this version posted April 16, 2021. The copyright holder for this preprint (which was not certified by peer review) is the author/funder, who has granted bioRxiv a license to display the preprint in perpetuity. It is made available under aCC-BY-NC-ND 4.0 International license.

332 identified to those of Zapata *et al.* (2016) (mapping and SV detection tools and parameters
333 being the same). Although the local variations cannot be comparable due to genome sequence
334 accuracy (complete genome *vs* whole genome sequencing) and the SV filtering differences (no
335 size filter *vs* > 1 kb), the majority of events are shared by the both studies.
336 Comparing locations of the L*er*-1 ONT SVs with Araport11 annotations, we found that
337 common and specific ONT SVs were preferentially linked to TE features and genes, as reported
338 in Jiao *et al* (2020). Looking at the GO-term enrichment in genes overlapping common ONT
339 SVs, an overrepresentation in defense response and ADP-binding terms corresponding to
340 resistance genes was observed. This result is concordant with previous studies
341 [13,24,44,63,64,65] in which an association between structural variations and the cluster
342 organisation of resistance genes was described.
343

344 ## General conclusion

345 Because analyses of SVs and their consequences heavily relies on the quality of their
346 identification and the underlying assembly/mapping data, we aimed to compare the
347 performance of ONT and Bionano biotechnologies for structural variation detection. Applying
348 stringent filters on ONT assembly mapping approach and size filters on SVs, we have shown
349 this methodology is an easy and efficient way to detect reliable SVs. Most of detected SVs were
350 also identified with Bionano optical maps with high concordancy despite different characteristic
351 (average, size, median). Nevertheless, long read sequencing technologies makes possible to
352 detect SVs more accurately, while Bionano offers a broad overview of structural
353 rearrangements. In addition, whole genome SVs analyses is currently mostly limited to model
354 organisms. However, because both Oxford Nanopore long reads and Bionano Genomics maps
355 assemblies do not require previous knowledge on genomic architecture or sequence of the

bioRxiv preprint doi: https://doi.org/10.1101/2021.04.16.440130; this version posted April 16, 2021. The copyright holder for this preprint (which was not certified by peer review) is the author/funder, who has granted bioRxiv a license to display the preprint in perpetuity. It is made available under aCC-BY-NC-ND 4.0 International license.

356 studied taxa, this approach expands the field of suitable plant species or species complexes
357 where in-depth SVs analyses can be performed.
358 Thereby, ONT appears to be especially suitable for SV studies in population or species
359 complex, and Bionano more relevant for characterization of genome specificity and genome
360 evolution, leading to an obvious complementarity of these two technologies in SVs analyses.
361

362 Methods

363 Plants

364 *Arabidopsis thaliana* Columbia-0 (accession number 186AV) and Landsberg *erecta*-1
365 (accession number 213AV) seeds were obtained from the Versailles Arabidopsis Stock Center,
366 INRAE. They were sown directly in soil and transplanted after 10 days. Plantlets were grown
367 under a 16h light/8 h night photoperiod in a growth chamber at 20°C for 4-5 weeks. Prior to
368 harvest, the plants were dark-treated for 3 days.

369 Oxford Nanopore Sequencing (MinION) HMW DNA extraction

370 High Molecular Weight (HMW) DNA extraction was performed using a modified salting-out
371 protocol. A total of 5g of freshly harvested leaves was ground in liquid nitrogen with a mortar
372 and pestle and transferred to 10ml of 50°C prewarmed extraction buffer in a 50ml tube
373 containing 1.25% SDS, 100mM Tris-HCl, pH 8, 50mM EDTA, 0.01% w/v PVP40. Then 37.5µl
374 of beta-mercaptoethanol (0.375% final) and 10µl RNAse A (Qiagen® 100mg/mL) were added.
375 This solution was incubated for 30 min at 50°C, under agitation (10 sec at 300rpm every 10
376 min). After incubation, 20ml TE (10:1) were added, slowly homogenized then 10ml of KAc
377 5M. The tube was kept on ice for 5 minutes, then centrifuged at 4°C during 10 min at 5000g.
378 The solution was transferred in two 15ml tubes and centrifuged again as previously. The
379 supernatant was transferred in a 50ml tube contening 1 volume of Isopropanol, slowly inverted
380 10 times, then centrifuged at 4°C for 10min at 500g. Pellets were washed with 20ml ethanol

bioRxiv preprint doi: https://doi.org/10.1101/2021.04.16.440130; this version posted April 16, 2021. The copyright holder for this preprint (which was not certified by peer review) is the author/funder, who has granted bioRxiv a license to display the preprint in perpetuity. It is made available under aCC-BY-NC-ND 4.0 International license.

381 70% then centrifuged at 4°C for 5 min at 500g. Supernatant was removed and pellets were not
382 completely dried before solubilization in 100µl of TE (10:1) prewarmed at 50°C. The DNA
383 solution was then incubated at 50°C for 10 min. Field Inverted Gel Electrophoresis (Program
384 50-150 kb on *Pipin Pulse* from Sage Science) was used for DNA size estimation and DNA
385 samples with molecule size above 50 kb were kept. Purity of DNA was evaluated by
386 spectrophotometry (OD260/280 and OD260/230 ratio).

387 **Bionano Optical Maps ultra HMW DNA extraction**

388 We performed the DNA extraction using the Base protocol n°30068 vD (Bionano Genomics)
389 with minor adaptations. Three grammes of very young fresh leaves from each genotype were
390 harvested from the dark-treated rosettes. The samples were placed on aluminium foil on ice
391 then transferred to a 50ml tube surrounded by a screened cap allowing pouring without lost of
392 samples (Bio-Rad) The tubes were kept on ice during the nuclear isolation. Samples were
393 treated in fixing solution containing 2% formaldehyde under a fume hood then rinsed with
394 fixing solution without formaldehyde. Fixed-leaves were transferred to a square Petri dish with
395 4ml of Plant Homogenization Buffer plus (HB+ is HB supplemented with 1mM spermine
396 tetrahydrochloride, 1mM spermidine trihydrochloride, and 0.2% 2-mercaptoethanol). Entire
397 leaves were chopped with a razor blade in 2x2mm pieces then transferred to a new tube on ice
398 and 7.5ml HB+ is added. Using TissueRuptor (Qiagen) the 2x2mm pieces were blended for a
399 total of four cycles (20 sec at maximum speed then resting 30 sec). Plant homogenates were
400 filtered, first through a 100µm then to a 40µm cell strainer and volumes were adjusted to 45ml.
401 Nuclei were centrifuged at 3840g at 4°C during 20 min, supernatants were discarded. Nuclei
402 were gently re-suspended in residual buffer, 3ml of HB+ were added, then tubes were swirled
403 on ice and the volumes were adjusted to 35ml. Homogenates were centrifuged at 60g at 4°C
404 during 3 min using minimum deceleration. Solutions were very carefully transferred to a new
405 tube in order to avoid carry-over of debris, and filtered again through a 40µm cell strainer.

bioRxiv preprint doi: https://doi.org/10.1101/2021.04.16.440130; this version posted April 16, 2021. The copyright holder for this preprint (which was not certified by peer review) is the author/funder, who has granted bioRxiv a license to display the preprint in perpetuity. It is made available under aCC-BY-NC-ND 4.0 International license.

406 Nuclei were centrifuged at 3840g at 4°C during 20 min, 3ml of HB+ were added and tubes were
407 swirled on ice. Using Bionano Nuclei Purification by Density Gradient, nuclei homogenate
408 were laid on the top of two solutions with different densities. After a 4500g centrifugation at
409 4°C during 40 min, the nuclei are at the interface of the two solutions. There are recovered with
410 a wide-bore tip in about 1ml solution and transferred in a 15ml tube and adjusted to 14ml with
411 HB+. Nuclei were centrifuged at 2500g at 4°C during 15 min. All the buffer were removed and
412 nuclei were re-suspended in 60µl HB+.
413 The nuclei solution were adjusted to 43°C for 3 min and melted 2% agarose from CHEF
414 Genomic DNA Plug Kits (Bio-Rad) was added to reach a 0.82% agarose plug concentration.
415 Plugs were cooled on aluminum blocks refrigerated on ice. Purification of the plugs was
416 performed with Bionano Lysis Buffer adjusted to pH 9 and supplemented with proteinase K
417 and 0.4% 2-mercaptoethanol. Plugs were digested during 2h at 50°C in Thermomixer then
418 solution were refreshed and incubated again overnight. Plugs were treated at RNAse for 1h at
419 37°C in remaining solution. Plugs were washed three times in Wash Buffer (Bionano
420 Genomics) then four times in TE 10:1. DNA retrieval was performed as recommended by
421 Bionano Genomics, as follow: plugs were melted at 70°C during 2 min then transferred
422 immediately at 43°C and incubated 45 min at 43°C with 2µl Agarase (0.5 unit/µl). The melted
423 plugs were recovered with wide-bore tips and dialyzed on a 0.1µm membrane disk (Millipore)
424 floating on 10ml TE for 1h. DNA was quantified in triplicates with Qubit according to Bionano
425 protocol. Two methods were used to estimate size of DNA molecules: *Pipin Pulse* and the
426 Qcard Argus System (Opgen) which allows DNA combing on a lane and visualization of
427 molecules after staining under fluorescent microscope. Samples with molecules above 150 kb
428 were kept for labeling. Protocols were performed according to Bionano Genomics with 600ng
429 of DNA for both Col-0 and L*er*-1 ecotypes. The direct label and stain (DLS) labeling consisted
430 in a single enzymatic labelling reaction with DLE-1 enzyme following by DNA staining with

bioRxiv preprint doi: https://doi.org/10.1101/2021.04.16.440130; this version posted April 16, 2021. The copyright holder for this preprint (which was not certified by peer review) is the author/funder, who has granted bioRxiv a license to display the preprint in perpetuity. It is made available under aCC-BY-NC-ND 4.0 International license.

431 a fluorescent marker. It was performed with 750ng DNA. Chip loading was performed as
432 recommended by Bionano Genomics.

433 **ONT Sequencing (MinION) and assembly**

434 ONT libraries were prepared according to the following protocol, using the Oxford Nanopore
435 SQK-LSK109 kit. Genomic DNA or DNA previously fragmented to 50 kb with a Megaruptor
436 (Diagenode S.A., Liege, Belgium) was first size-selected using a BluePippin (Sage Science,
437 Beverly, MA, USA). The selected DNA fragments were end-repaired and 3'-adenylated with
438 the NEBNext® Ultra™ II End Repair/dA-Tailing Module (New England Biolabs, Ipswich,
439 MA, USA). The DNA was then purified with AMPure XP beads (Beckmann Coulter, Brea,
440 CA, USA) and ligated with sequencing adapters provided by Oxford Nanopore Technologies
441 (Oxford Nanopore Technologies Ltd, Oxford, UK) using Blunt/TA Ligase Master Mix (NEB).
442 After purification with AMPure XP beads, the library was mixed with Running Buffer with
443 Fuel Mix (ONT) and Library Loading Beads (ONT) and loaded on 4 MinION R9.4 SpotON
444 Flow Cells per *Arabidopsis thaliana* ecotypes. Resulting FAST5 files were base-called using
445 albacore (versions 2.1.10 and 2.3.1) and FASTA produced as described in Istace *et al* (2017).
446 Canu version 1.5 (github commit ae9eecc), was used for initial read correction and trimming
447 with the parameters minMemory=100G, corOutCoverage = 10000. The corrected sequences
448 were merged in one final FASTA file per ecotype that were later used as assemblers input.
449 Assemblies were performed with the relevant genome size parameter set to, or coverage
450 calculation based on, a 130 Mb genome size. Assemblers used with default parameters were
451 Canu version 1.5 ([56], github commit 69b5f32), Rapid Assembler (RA, https://github.com/lbcb-
452 sci/ra commit 07364a1) and SMARTdenovo version 1.0 (with the option –c 1 to run the
453 consensus step) (https://github.com/ruanjue/smartdenovo commit 61cf13d). The MUMmer
454 suite version 3.0 [59] was run with the parameters used in Zapata *et al*. 2016. To analyze the
455 assemblies, they were aligned to the reference genome of *Arabidopsis thaliana* Columbia 0

bioRxiv preprint doi: https://doi.org/10.1101/2021.04.16.440130; this version posted April 16, 2021. The copyright holder for this preprint (which was not certified by peer review) is the author/funder, who has granted bioRxiv a license to display the preprint in perpetuity. It is made available under aCC-BY-NC-ND 4.0 International license.

456 (Col-0, TAIR10.1 GCF_000001735.4) and the sequence of *Arabidopsis thaliana* Landsberg
457 *erecta* (L*er*, Genbank LUHQ00000000.1) using *nucmer* with the options -c 100 -b 500 -l 50 -g
458 100 -L 50. The alignments were filtered with *delta-filter* (options -1 -l 10000 -i 0.95) and
459 visualized with the *mummer-plot* (options --fat --large --layout --png) or DNAnexus (github
460 commit 78e3317). These MUMmer parameters [44] allowed conserving exact matches larger
461 than 50bp and alignments longer than 10 kb with a minimal identity of 95%. To check
462 assemblies' completeness and fragmentation, they were compared to each other based on the
463 metrics (Number of contigs, N50, cumulative genome sizes) and the genome alignments to the
464 references generated with MUMmer viewed with the DNAnexus dot
465 (https://dnanexus.github.io/dot/).
466 To evaluate the completness of our ONT data, mapping of the corrected ONT reads on the Col-
467 0 TAIR10.1 reference were performed with Minimap2/2.15 aligner [57] with -a -x map-ont
468 parameters. The Samtools/1.6 depth tool with –a option [66] gave us the alignement depth at
469 each Col-0 TAIR10.1 reference positions.

470 **Bionano Optical Map assembly**

471 As it can be beneficial for assembly steps, molecules sub-sampling was conducted when
472 flowcells yielded more than 90 Gb and 600X of data. This adapted selection of molecules was
473 made on each run with the Bionano RefAligner tool in command line (version 1.3.8041.8044
474 with –minlen 180 –randomize 1 –subset 1 nb_molec options) or with Bionano Access (version
475 Solve3.3 with Filter Molecule Object utility) (Additional file 1: Tables S6 and S7).
476 Maps were then constructed with the tool *Generate de novo Assembly* of the Bionano Solve
477 (version 3.3) using the options recommended by Bionano (With pre-assembly, Non haplotype
478 without extend and split) and a 0.115 Gb genome size. The pre-assembly step calculates noise
479 parameters that optimizes the quality of the assembly (less and larger maps). When a reference
480 FASTA file is added, noise parameters are calculated in aligning the molecules to the reference.

bioRxiv preprint doi: https://doi.org/10.1101/2021.04.16.440130; this version posted April 16, 2021. The copyright holder for this preprint (which was not certified by peer review) is the author/funder, who has granted bioRxiv a license to display the preprint in perpetuity. It is made available under aCC-BY-NC-ND 4.0 International license.

481 Otherwise, the noise parameters are estimated thanks to a first rough assembly of the molecules.
482 For Col-0 and L*er*-1 ecotypes, three maps were obtained, one without reference, one with the
483 Col-0 reference and one with the L*er* reference (Additional file 1: Tables S8 and S9). In our
484 study, the metrics of these assemblies are very similar. This stability reflects that noise
485 parameters estimated either with references fasta sequences or our data, were comparable. This
486 is a guaranty of quality of Bionano data and assemblies.

487 **ONT variation detection**

488 Structural variations were obtained with MUMmer's show-diff utility on the filtered alignments
489 of SMARTdenovo assemblies against the references Col-0 and L*er*. One DIFF file per
490 comparison were obtained. Six SV types (Gap, Duplication, Break, Jump, Inversion, Sequence)
491 were described in the Additional file 2: Figure S4.

492 **Bionano variation detection**

493 SVs detections were performed on the optical maps built with the public reference and our
494 SMARTdenovo ONT assemblies using the tool Convert SMAP to VCF file. VCF files were
495 recovered, describing all the structural variations between the optical maps and the considered
496 reference. The variations were classified in 6 types: deletion, insertion, translocation and
497 inversion. SVs detection stringency is intrinsic, based on the number of aligned molecules (at
498 least nine by default) and the number of labels accross each variants breakpoint on the genome
499 map (at least two by default) (Bionano tutorial : https://bionanogenomics.com/support-
500 page/data-analysis-documentation/). The technology gave an interval with an uncertainty about
501 breakpoint positions (CIPOS and CIEND in VCF files). In this study, these values were used
502 to calculate the most extended positions for the Bionano SVs and avoid effect of label fluzz.
503 The low number of structural variations between Col-0 optical maps and the Col-0 TAIR10.1
504 reference (as L*er*-1 maps and L*er* reference) reflects the good collinearity between the map and
505 the references. SVs gave us an indication on location of conflicts that could be due to mis-

bioRxiv preprint doi: https://doi.org/10.1101/2021.04.16.440130; this version posted April 16, 2021. The copyright holder for this preprint (which was not certified by peer review) is the author/funder, who has granted bioRxiv a license to display the preprint in perpetuity. It is made available under aCC-BY-NC-ND 4.0 International license.

506 assemblies or intra-ecotype variations. Inter-ecotype detection allowed us to describe the
507 variations between Col-0 and L*er*-1.
508 Quality and length characteristics were used to better describe and filter SVs. Bionano Solve
509 associates a quality score to each INS and DEL based on sensitivity and the fraction of
510 alternative calls in mix assemblies that were called in the alternative genome assembly [from
511 no quality (.) or poor (0) to confident quality (20)]. We observed that this indicator follows the
512 same trend as the SVs size (Additional file 1: Tables S11 and S15). Moreover, size range values
513 where SVs abundances are the most different between both technologies are the extremes : the
514 smallest (< 1 kb), where ONT technology detected much more SVs and the highest (> 5 kb)
515 where Bionano technology detected proportionnally more SVs. So in our comparison analysis,
516 to remove poor quality Bionano SVs, ONT sequencing errors and high sensitivity, a filter on
517 query SV size (> 1 kp) was applied. Confidence scores for translocation and inversion
518 breakpoints were computed as p-values, giving true confidence (in Mahalanobis distance) to
519 positive calls. The recommended cutoffs are 0.1 and 0.01 for translocation and inversion
520 breakpoints calls respectively and were used to eliminate uncertain inversion on Chr2.

521 **SV description**

522 Custom-made R and Perl scripts were used to edit other tools outputs, describe ONT and
523 Bionano SVs (types, size), locate SVs along the chromosomes and filter them. For ONT
524 technology, SVs identified as assemblies discordances were quickly described and discarded
525 before comparison. Those included sequences (SEQ), breaks (BRK) and jumps (JMP) ONT SV
526 because they correspond to assembly or reference artefacts. Finally, size filters (more than 1
527 kb) were applied to take into accountONT high sequencing error rate, and low quality Bionano
528 SVs. For Bionano SVs the largest absolute positions of the SV were conserved, taking into
529 account the uncertainty around breakpoints due to the distance between two labels.

530 **SV comparison**

bioRxiv preprint doi: https://doi.org/10.1101/2021.04.16.440130; this version posted April 16, 2021. The copyright holder for this preprint (which was not certified by peer review) is the author/funder, who has granted bioRxiv a license to display the preprint in perpetuity. It is made available under aCC-BY-NC-ND 4.0 International license.

531 Comparison of SV obtained with both ONT and Bionano technologies were based on the
532 overlap of their absolute positions.
533 ONT SV and Bionano SVs files were used after conversion to BED format to identify
534 overlapping regions with BEDtools (version 2.27.1, github commit cd82ed5, "bedtools
535 intersect -wa -wb -a INPUT1.bed -b INPUT2.bed -loj > OUTPUT.bed"). Raw comparisons
536 were then compared, compiled and formatted in one final output file using custom-made R
537 scripts. For each SVs location, this file contained descriptors (SVs size, type, quality) for both
538 technologies, information on the type of conflict and a 2 letter code. This code characterized
539 the SVs location as follow : the first letter corresponds to the ONT SV characterization, the
540 second to the Bionano SV. M ("Multiple") means more than one SV, U ("Unique") one SV, N
541 ("None") no SV. For example, the code "MU" means that this location arbored multiple ONT
542 SV corresponding to a unique Bionano. The landscapes and SVs occurences visualization was
543 performed with Circos/0.69.9 tool (perl/5.16.3) [67].

544 **SV and annotation**

545 SVs overlapping a gene and/or TE were identified with the bedtools intersect by comparing
546 their absolute positions to *A. thaliana* Col-0 annotations (11th july 2019 release,
547 TAIR10_GFF3_genes_transposons.gff). Lists of genes impacted by SV for both technologies
548 were extracted and a GO-term enrichment analysis performed using Fisher's Exact test with a
549 Bonferroni correction in PANTHER (released 20200407 with GO Ontology database DOI:
550 10.5281/zenodo.3873405 Released 2020-06-01, [61], http://go.pantherdb.org/). Significance
551 was evaluated based on a P-value $\leq 10-5$ and an FDR value ≤ 0.01 [67].

552

553

554

555

bioRxiv preprint doi: https://doi.org/10.1101/2021.04.16.440130; this version posted April 16, 2021. The copyright holder for this preprint (which was not certified by peer review) is the author/funder, who has granted bioRxiv a license to display the preprint in perpetuity. It is made available under aCC-BY-NC-ND 4.0 International license.

556 ## List of abbreviations

557 If abbreviations are used in the text they should be defined in the text at first use, and a list of
558 abbreviations can be provided.

559 bp base pairs

560 BRK Break

561 CGH Comparative Genomic Hybridization

562 CNV copy number variations

563 Col-0 *Arabidopsis thaliana* ecotypes Columbia-0

564 DEL Deletion

565 DLE-1 Direct Label Enzyme – 1

566 DLS Direct Label and Stain

567 DNA Desoxyribo Nucleic Acid

568 DUP Duplication

569 Gb Gigabases

570 Hi-C HIgh-throughput chromatin conformation Capture

571 Indels insertions/deletions

572 INS Insertion

573 INV Inversion

574 JMP Jump

575 Kb kilobases

576 L*er*-1 *Arabidopsis thaliana* ecotypes Landsberg *erecta* 1

577 LER *Arabdopsis thaliana* L*er*-1 reference genome published by Zapata *et al*. 2016.

578 NA Not Available

579 NGS Next Generation Sequence

580 ONT Oxford Nanopore Technologies

bioRxiv preprint doi: https://doi.org/10.1101/2021.04.16.440130; this version posted April 16, 2021. The copyright holder for this preprint (which was not certified by peer review) is the author/funder, who has granted bioRxiv a license to display the preprint in perpetuity. It is made available under aCC-BY-NC-ND 4.0 International license.

581 PAV presence/absence variations

582 RA Rapid Assembler

583 SDN SMARTdenovo

584 SEQ Sequence

585 SNP Single Nucleotid Polymorphism

586 SV Structural Variation

587 TAIR10.1 last version of *Arabdopsis thaliana* Col-0 reference genome availbale at the The

588 Arabidopsis Information Resource repository (TAIR).

589 TE Transposable Element

590 TRA Translocation

591

592

593

594

595

596

597

598

599

600

601

602

603

604

605

bioRxiv preprint doi: https://doi.org/10.1101/2021.04.16.440130; this version posted April 16, 2021. The copyright holder for this preprint (which was not certified by peer review) is the author/funder, who has granted bioRxiv a license to display the preprint in perpetuity. It is made available under aCC-BY-NC-ND 4.0 International license.

606 # Figure description

607 **Figure 1**. Circos visualization of L*er*-1 SVs landscape.

608 All comparisons were performed against the Col-0 TAIR10.1 reference sequence per 100kb
609 bins. From external to internal layer :
610 Col-0 TAIR10.1 chromosomes (ticks every 100 kb) : black and light grey rectangles represent
611 centromeric and NOR regions respectively;
612 Average mapping coverage for Col-0 ONT reads (grey line) and L*er*-1 ONT reads (orange line
613 with dark orange if coverage > 46X);
614 DLE-1 label density as purple line (dark purple if density > 18 label per 100 kb);
615 Genes density as green line (dark green if density > 23), NLR Genes [68] indicated as green
616 rectangles;
617 TEs density as blue line (dark blue if density > 58);
618 ONT SVs occurences as orange outwards bars (dark orange bars represent ONT- specific SVs);
619 Bionano SVs occurrences as purple inwards bars (dark purple bars represent Bionano-specific
620 SVs).
621

622 # Additional files description :

623 **Additional_file_1.xlsx : Additional tables results**

624 Table S1. Metrics of the ONT run flowcells for *A. thaliana* Columbia (Col-0).
625 Note : All sizes are in base pairs. ALL_COL is all Col-0 trimmed merged data.
626 Table S2. Metrics of the ONT run flowcells for *A. thaliana* Landsberg *erecta* (L*er*-1). All sizes
627 are in base pairs.
628 Note : All sizes are in base pairs. ALL_LER is all L*er*-1 trimmed merged data.
629 Table S3. Number of the Col-0 TAIR10.1 and L*er* references bases covered and uncovered by
630 ONT reads.

bioRxiv preprint doi: https://doi.org/10.1101/2021.04.16.440130; this version posted April 16, 2021. The copyright holder for this preprint (which was not certified by peer review) is the author/funder, who has granted bioRxiv a license to display the preprint in perpetuity. It is made available under aCC-BY-NC-ND 4.0 International license.

631 Note : ONT reads are *A. thaliana* Col-0 and L*er*-1 corrected, trimmed and merged ONT
632 sequences (respectively ALL_COL and ALL_LER).
633 Table S4. *A. thaliana* Col-0 Assembly Metrics for contigs only, obtained with SMARTdenovo,
634 Canu and RA.
635 Note : All sizes are in base pairs. Assemblies are obtained with corrected, trimmed and merged
636 Col-0 ONT sequences.
637 Table S5. *A. thaliana* L*er*-1 Assembly Metrics for contigs only, obtained SMARTdenovo, Canu
638 and RA.
639 Note : All sizes are in base pairs. Assemblies are obtained with corrected, trimmed and merged
640 L*er*-1 sequences.
641 Table S6. Metrics of the Bionano run chips for *A. thaliana* Columbia (Col-0) and Landsberg
642 *erecta* (L*er*-1).
643 Note : All sizes are in base pairs. Results obtained with DLE-1 labelling.
644 Table S7. Metrics of the sampled Bionano run chips for *A. thaliana* Columbia (Col-0) and
645 Landsberg *erecta* (L*er*-1).
646 Note : All sizes are in base pairs. Results obtained with DLE-1 labelling.
647 Table S8. Assembly Metrics of *A. thaliana* Columbia (Col-0) sampled molecules.
648 Note : The options used were "Pre-assembly", "Non Haplotype" and "Without Extend and
649 Split".
650 Table S9. Assembly Metrics of *A. thaliana* Landsberg *erecta* (L*er*-1) sampled molecules.
651 Note : The options used were "Pre-assembly", "Non Haplotype" and "Without Extend and
652 Split".
653 Table S10.Types of Col-0 ONT and Bionano SVs obtained against L*er* reference.
654 Table S11. Size repartition of Col-0 ONT and Bionano insertions, deletions, INVersions,
655 translocations obtained against L*er* reference.

bioRxiv preprint doi: https://doi.org/10.1101/2021.04.16.440130; this version posted April 16, 2021. The copyright holder for this preprint (which was not certified by peer review) is the author/funder, who has granted bioRxiv a license to display the preprint in perpetuity. It is made available under aCC-BY-NC-ND 4.0 International license.

656 Table S12. Characteristics of Evry.Col-0 ONT and Bionano SVs, obtained after alignement
657 against L*er* reference.
658 Table S13. Characteristics of compared ONT Col-0 SVs with query size > 1kb.
659 Table S14. Characteristics of compared Bionano Col-0 SVs with query size > 1kb.
660 Table S15. Size repartition of L*er*-1 ONT and Bionano insertions and deletions obtained against
661 Col-0 TAIR10.1 reference.
662 Table S16. Characteristics of compared ONT L*er*-1 SVs with query size > 1kb.
663 Table S17. Characteristics of compared Bionano L*er*-1 SVs with query size > 1kb.
664 Table S18.Genes overlapping L*er*-1 SV in common locations (query size >1 kb).
665 Table S19. Gene annotation overlapping L*er*-1 SV in common locations (query size >1kb).
666 Note : PANTHER released 20200407 was used with GO Ontology database DOI:
667 10.5281/zenodo.3873405 Released 2020-06-01, [61], http://go.pantherdb.org/).
668 Table S20. PANTHER Overrepresentation results on Genes overlapping common L*er*-1 SVs
669 (query size >1kb).
670 Note : The PANTHER version is decribed in Mi *et al*. 2019.
671 Table S21. Genes overlapping specific ONT L*er*-1 SVs (query size >1 kb).
672 Table S22. Gene annotation overlapping specific ONT L*er*-1 SVs (query size >1kb).
673 Note : PANTHER released 20200407 was used with GO Ontology database DOI:
674 10.5281/zenodo.3873405 Released 2020-06-01, [61], http://go.pantherdb.org/).
675 Table S23. PANTHER Overrepresentation results on Genes overlapping specific ONT L*er*-1
676 SVs (query size >1 kb).
677 Note : The PANTHER version is decribed in Mi *et al*. 2019
678

679 **Additional_file_2.pdf : Additional figures results :**

680 Figure S1A-C. Views of Col-0 contigs alignments on Col-0 TAIR10.1 reference (dotted end).

bioRxiv preprint doi: https://doi.org/10.1101/2021.04.16.440130; this version posted April 16, 2021. The copyright holder for this preprint (which was not certified by peer review) is the author/funder, who has granted bioRxiv a license to display the preprint in perpetuity. It is made available under aCC-BY-NC-ND 4.0 International license.

681 (A) Contigs obtained with SMARTdenovo, (B) with Canu and (C) with RA. Blue, green and
682 orange dots and lines represent unique forward, unique reverse and repetitive alignments
683 respectively.
684 Figure S2A-C. Views of L*er*-1 contigs alignments on L*er* reference (dotted end).
685 (A) Contigs obtained with SMARTdenovo, (B) with Canu and (C) with RA. Blue, green and
686 orange dots and lines represent unique forward, unique reverse and repetitive alignments
687 respectively.
688 Figure S3A-E. Bionano Access view of L*er*-1 cmaps aligned on Col-0 TAIR10.1 reference.
689 (A) to (E) are alignments on Col-0 TAIR10.1 Chr1 to Chr5. Maps are in green for the Col-0
690 TAIR10.1 reference and light blue for L*er*-1 genome with the molecules depth curve in blue.
691 Consistant DLE-1 enzyme label between reference and L*er*-1 maps are represented with dark
692 blue bars with grey links between the genomes maps. Inconsistant DLE-1 enzyme label are
693 yellow bars on the two genomes maps.
694 Figure S4. Description of SVs detected by MUMmer show-diff and Bionano Access tools.
695 Insertion in the query are called GAP with a negative size by MUMmer show-diff, INS by
696 Bionano Access. Deletion in the query are called GAP with a positive size by MUMmer show-
697 diff, DEL by Bionano Access. Inversion in the query are called INV by MUMmer show-diff
698 and Bionano Access. Duplication in the query are called DUP by MUMmer show-diff and by
699 Bionano Access. Rearrangement of reference sequence in the query are called jump (JMP) by
700 MUMmer show-diff and translocation (TRA) by Bionano Access. Inverted Duplication are not
701 described by MUMmer show-diff and called INVDUP by Bionano Access. Reference sequence
702 junction between two assemblies contigs alignment are called SEQ by MUMmer show-diff and
703 are not described by Bionano Access. Query sequence junction between two reference
704 chromosomes alignment are called break (BRK) by MUMmer show-diff and are not described
705 by Bionano Access. « - » means no detection with the technology.

bioRxiv preprint doi: https://doi.org/10.1101/2021.04.16.440130; this version posted April 16, 2021. The copyright holder for this preprint (which was not certified by peer review) is the author/funder, who has granted bioRxiv a license to display the preprint in perpetuity. It is made available under aCC-BY-NC-ND 4.0 International license.

706 Figure S5A-E. Col-0 SVs (>1kb) occurences.

707 All comparisons were performed against the L*er* reference sequence per 100kb bins and black
708 rectangles symbolize L*er* centromeric regions. Average mapping coverage for Col-0 ONT reads
709 (red line called COV), average DLE-1 density labelling (green line called DLE), and ONT and
710 Bionano occurrences (rea and green bars respectively) are represented for each L*er*
711 chromosome in section A to E respectively for Chr1 to Chr5.

712 Figure S6. Bionano Solve zoom in the Chr2 L*er*-1 translocations against Col-0 TAIR10.1
713 reference.

714 Maps are in green for the Col-0 TAIR10.1 reference and light blue for L*er*-1 genome.
715 Consistant DLE-1 enzyme label between reference and L*er*-1 maps are represented with dark
716 blue bars with grey links between the genomes maps. Inconsistant DLE-1 enzyme label are
717 yellow bars on the two genomes maps. The purple bar locate the translocation events on the
718 Ler-1 map. The red box and lines highlight the zoom.

719 Figure S7. Bionano Solve capture of the L*er*-1 Chr4 extra-range Size Invertion against Col-0
720 TAIR10.1 reference.

721 Maps are in green for the Col-0 TAIR10.1 reference and light blue for L*er*-1 genome.
722 Consistant DLE-1 enzyme label between reference and L*er*-1 maps are represented with dark
723 blue bars with grey links between the genomes maps. Inconsistant DLE-1 enzyme label are
724 yellow bars on the two genomes maps. The red box and lines highlight the zoom.

725

726 ## Declarations

727 **Ethics approval and consent to participate**

728 Not applicable.

729

730 **Consent for publication**

bioRxiv preprint doi: https://doi.org/10.1101/2021.04.16.440130; this version posted April 16, 2021. The copyright holder for this preprint (which was not certified by peer review) is the author/funder, who has granted bioRxiv a license to display the preprint in perpetuity. It is made available under aCC-BY-NC-ND 4.0 International license.

731 Not applicable.

732

733 **Availability of data and materials**

734 The ONT reads files and the Bionano molecules files have been submitted to the European
735 Nucleotide Archive (http://www.ebi.ac.uk) and are publicly available with the accession
736 numbers ERP128342 and ERZ1959921 respectively. Assemblies and optical maps of the Col-
737 0 and L*er*-1 genomes are publicly available in separate ENA studies under the accession number
738 PRJEB44316.

739

740 **Competing interests**

741 The authors declare that they have no competing interests.

742

743 **Funding**

744 This work was supported by INRAE (Institut National de Recherche pour l'Agriculture,
745 l'alimentation l'Environnement) and Genoscope-CEA (Commissariat à l'Energie Atomique et
746 aux Energies Alternatives).

747

748 **Authors' contributions**

749 The project was conceived by VB, MCLP and PFR. Plant cultures and the HMW DNA
750 extraction for Oxford Nanopore and Bionano Technologies were carried out by ED and GM,
751 data acquisition by ED, GM, CC, CB, BI and equipment provided by PW, MCLP, PFR, VB.
752 Data analysis were performed by AC, BI and CB for assemblies, optical maps and SV detection
753 and AC and RG for SV comparisons. PFR, VB contributed to data interpretation with AC and
754 RG. The manuscript was written by AC, RG, PFR, VB with inputs from PW and MCLP. All
755 authors read and approved the final manuscript.

bioRxiv preprint doi: https://doi.org/10.1101/2021.04.16.440130; this version posted April 16, 2021. The copyright holder for this preprint (which was not certified by peer review) is the author/funder, who has granted bioRxiv a license to display the preprint in perpetuity. It is made available under aCC-BY-NC-ND 4.0 International license.

756

757 **Acknowledgements**

758 The authors would like to thank the Versailles *Arabidopsis* Stock Center, INRAE providing
759 *Arabidopsis thaliana* ecotypes and the Institut of Plant Sciences Paris Saclay (IPS2) where the
760 *Arabidopsis* cultures were carried out.
761 We also greatly thank Damien Hinsinger for proofreading and advice on the manuscript and
762 the INRAE PepiAnnot Group (https://pepi-ibis.inra.fr/annotation-genomes) for helpful
763 discussions.

764

765 **Authors' information**

766 [1] Université Paris-Saclay, INRAE, Etude du Polymorphisme des Génomes Végétaux (EPGV),
767 91000, Evry-Courcouronnes, France.
768 [2] Génomique Métabolique, Genoscope, Institut François Jacob, CEA, CNRS, Univ Evry,
769 Université Paris-Saclay, 91057 Evry, France.
770 [3] Genoscope, Institut de biologie François-Jacob, Commissariat à l'Energie Atomique (CEA),
771 Université Paris-Saclay, Evry, France.
772 *Corresponding author: Patricia Faivre Rampant
773 aurelie.canaguier@inrae.fr
774 romane.guilbaud@inrae.fr
775 erwandenis@hotmail.com
776 gmagdele@genoscope.cns.fr
777 cbelser@genoscope.cns.fr
778 bistace@genoscope.cns.fr
779 cruaud@genoscope.cns.fr
780 marie-christine.le-paslier@inrae.fr
781 pwincker@genoscope.cns.fr

bioRxiv preprint doi: https://doi.org/10.1101/2021.04.16.440130; this version posted April 16, 2021. The copyright holder for this preprint (which was not certified by peer review) is the author/funder, who has granted bioRxiv a license to display the preprint in perpetuity. It is made available under aCC-BY-NC-ND 4.0 International license.

782

783 patricia.faivre-rampant@inrae.fr

784 vbarbe@genoscope.cns.fr

785

786 **Footnotes**

787 Not applicable.

788

789

790 **References**

791 1. Saxena RK, Edwards D, Varshney RK. Structural variations in plant genomes. Brief Funct
792 Genomics. 2014 Jul;13(4):296–307.
793 2. Escaramís G, Docampo E, Rabionet R. A decade of structural variants: description, history and
794 methods to detect structural variation. Brief Funct Genomics. 2015 Sep 1;14(5):305–14.
795 3. Zhang X, Chen X, Liang P, Tang H. Cataloging Plant Genome Structural Variations. Current Issues
796 in Molecular Biology. 2018;181–94.
797 4. Ho SS, Urban AE, Mills RE. Structural variation in the sequencing era. Nature Reviews Genetics.
798 2020 Mar;21(3):171–89.
799 5. Wendel JF, Jackson SA, Meyers BC, Wing RA. Evolution of plant genome architecture. Genome
800 Biol. 2016 Dec;17(1):1–14.
801 6. Gabur I, Chawla HS, Snowdon RJ, Parkin IAP. Connecting genome structural variation with
802 complex traits in crop plants. Theor Appl Genet. 2019 Mar 1;132(3):733–50.
803 7. Schiessl S-V, Katche E, Ihien E, Chawla HS, Mason AS. The role of genomic structural variation in
804 the genetic improvement of polyploid crops. The Crop Journal. 2019 Apr;7(2):127–40.
805 8. Voichek Y, Weigel D. Identifying genetic variants underlying phenotypic variation in plants
806 without complete genomes. Nat Genet. 2020 May;52(5):534–40.

bioRxiv preprint doi: https://doi.org/10.1101/2021.04.16.440130; this version posted April 16, 2021. The copyright holder for this preprint (which was not certified by peer review) is the author/funder, who has granted bioRxiv a license to display the preprint in perpetuity. It is made available under aCC-BY-NC-ND 4.0 International license.

807 9. Muñoz-Amatriaín M, Eichten SR, Wicker T, Richmond TA, Mascher M, Steuernagel B, et al.
808 Distribution, functional impact, and origin mechanisms of copy number variation in the barley
809 genome. Genome Biol. 2013 Jun;14(6):R58.
810 10. Dolatabadian A, Patel DA, Edwards D, Batley J. Copy number variation and disease resistance in
811 plants. Theor Appl Genet. 2017 Dec 1;130(12):2479–90.
812 11. Fuentes RR, Chebotarov D, Duitama J, Smith S, De la Hoz JF, Mohiyuddin M, et al. Structural
813 variants in 3000 rice genomes. Genome Res. 2019;29(5):870–80.
814 12. Tao Y, Zhao X, Mace E, Henry R, Jordan D. Exploring and Exploiting Pan-genomics for Crop
815 Improvement. Molecular Plant. 2019 Feb 4;12(2):156–69.
816 13. Wei H, Liu J, Guo Q, Pan L, Chai S, Cheng Y, et al. Genomic Organization and Comparative
817 Phylogenic Analysis of NBS-LRR Resistance Gene Family in Solanum pimpinellifolium and
818 Arabidopsis thaliana. Evol Bioinform Online. 2020;16:1176934320911055.
819 14. Prunier J, Caron S, MacKay J. CNVs into the wild: screening the genomes of conifer trees (Picea
820 spp.) reveals fewer gene copy number variations in hybrids and links to adaptation. BMC
821 Genomics. 2017 Dec;18(1):97.
822 15. Prunier J, Giguère I, Ryan N, Guy R, Soolanayakanahally R, Isabel N, et al. Gene copy number
823 variations involved in balsam poplar (Populus balsamifera L.) adaptive variations. Mol Ecol. 2019
824 Mar;28(6):1476–90.
825 16. Wang Y, Xiong G, Hu J, Jiang L, Yu H, Xu J, et al. Copy number variation at the GL7 locus contributes
826 to grain size diversity in rice. Nature Genetics. 2015 Aug;47(8):944–8.
827 17. Gong C, Du Q, Xie J, Quan M, Chen B, Zhang D. Dissection of Insertion–Deletion Variants within
828 Differentially Expressed Genes Involved in Wood Formation in Populus. Front Plant Sci [Internet].
829 2018 [cited 2019 Aug 20];8. Available from:
830 https://www.frontiersin.org/articles/10.3389/fpls.2017.02199/full?report=reader
831 18. Gao L, Gonda I, Sun H, Ma Q, Bao K, Tieman DM, et al. The tomato pan-genome uncovers new
832 genes and a rare allele regulating fruit flavor. Nature Genetics. 2019 Jun;51(6):1044.

bioRxiv preprint doi: https://doi.org/10.1101/2021.04.16.440130; this version posted April 16, 2021. The copyright holder for this preprint (which was not certified by peer review) is the author/funder, who has granted bioRxiv a license to display the preprint in perpetuity. It is made available under aCC-BY-NC-ND 4.0 International license.

833 19. Tranchant-Dubreuil C, Rouard M, Sabot F. Plant Pangenome: Impacts On Phenotypes And
834 Evolution. Annual Plant Reviews [Internet]. 2019 May [cited 2021 Feb 11]; Available from:
835 https://hal.archives-ouvertes.fr/hal-02053647
836 20. Khan AW, Garg V, Roorkiwal M, Golicz AA, Edwards D, Varshney RK. Super-Pangenome by
837 Integrating the Wild Side of a Species for Accelerated Crop Improvement. Trends in Plant Science.
838 2020 Feb 1;25(2):148–58.
839 21. Li R, Li Y, Zheng H, Luo R, Zhu H, Li Q, et al. Building the sequence map of the human pan-genome.
840 Nature Biotechnology. 2010 Jan;28(1):57–63.
841 22. Sherman RM, Forman J, Antonescu V, Puiu D, Daya M, Rafaels N, et al. Assembly of a pan-genome
842 from deep sequencing of 910 humans of African descent. Nature Genetics. 2019 Jan;51(1):30–5.
843 23. Duan Z, Qiao Y, Lu J, Lu H, Zhang W, Yan F, et al. HUPAN: a pan-genome analysis pipeline for
844 human genomes. Genome Biology. 2019 Jul 31;20(1):149.
845 24. Jiao W-B, Schneeberger K. Chromosome-level assemblies of multiple Arabidopsis genomes reveal
846 hotspots of rearrangements with altered evolutionary dynamics. Nature Communications. 2020
847 Feb 20;11(1):989.
848 25. Song J-M, Guan Z, Hu J, Guo C, Yang Z, Wang S, et al. Eight high-quality genomes reveal pan-
849 genome architecture and ecotype differentiation of Brassica napus. Nat Plants. 2020 Jan;6(1):34–
850 45.
851 26. Springer NM, Ying K, Fu Y, Ji T, Yeh C-T, Jia Y, et al. Maize Inbreds Exhibit High Levels of Copy
852 Number Variation (CNV) and Presence/Absence Variation (PAV) in Genome Content. PLOS
853 Genetics. 2009 Nov 20;5(11):e1000734.
854 27. Swanson-Wagner RA, Eichten SR, Kumari S, Tiffin P, Stein JC, Ware D, et al. Pervasive gene
855 content variation and copy number variation in maize and its undomesticated progenitor.
856 Genome Res. 2010 Jan 12;20(12):1689–99.
857 28. Hwang JE, Kim S-H, Jung IJ, Han SM, Ahn J-W, Kwon S-J, et al. Comparative genomic hybridization
858 analysis of rice dwarf mutants induced by gamma irradiation. Genet Mol Res. 2016 Dec 23;15(4).

bioRxiv preprint doi: https://doi.org/10.1101/2021.04.16.440130; this version posted April 16, 2021. The copyright holder for this preprint (which was not certified by peer review) is the author/funder, who has granted bioRxiv a license to display the preprint in perpetuity. It is made available under aCC-BY-NC-ND 4.0 International license.

859 29. Gimode D, Odeny DA, de Villiers EP, Wanyonyi S, Dida MM, Mneney EE, et al. Identification of
860 SNP and SSR Markers in Finger Millet Using Next Generation Sequencing Technologies. PLoS ONE.
861 2016;11(7):e0159437.
862 30. Lyons E, Freeling M, Kustu S, Inwood W. Using Genomic Sequencing for Classical Genetics in E.
863 coli K12. PLoS One [Internet]. 2011 Feb 25 [cited 2020 May 15];6(2). Available from:
864 https://www.ncbi.nlm.nih.gov/pmc/articles/PMC3045373/
865 31. Brenchley R, Spannagl M, Pfeifer M, Barker GLA, D'Amore R, Allen AM, et al. Analysis of the bread
866 wheat genome using whole genome shotgun sequencing. Nature. 2012 Nov 29;491(7426):705–
867 10.
868 32. Xing L, Zhang D, Song X, Weng K, Shen Y, Li Y, et al. Genome-Wide Sequence Variation
869 Identification and Floral-Associated Trait Comparisons Based on the Re-sequencing of the
870 'Nagafu No. 2' and 'Qinguan' Varieties of Apple (Malus domestica Borkh.). Front Plant Sci
871 [Internet]. 2016 [cited 2020 May 11];7. Available from:
872 https://www.frontiersin.org/articles/10.3389/fpls.2016.00908/full
873 33. Maldonado dos Santos JV, Valliyodan B, Joshi T, Khan SM, Liu Y, Wang J, et al. Evaluation of
874 genetic variation among Brazilian soybean cultivars through genome resequencing. BMC
875 Genomics. 2016 Feb 13;17(1):110.
876 34. The 1001 Genomes Consortium, Alonso-Blanco C, Andrade J, Becker C, Bemm F, Bergelson J, et
877 al. 1,135 Genomes Reveal the Global Pattern of Polymorphism in Arabidopsis thaliana. Cell. 2016
878 Jul 14;166(2):481–91.
879 35. Pucker B, Holtgräwe D, Rosleff Sörensen T, Stracke R, Viehöver P, Weisshaar B. A De Novo
880 Genome Sequence Assembly of the Arabidopsis thaliana Accession Niederzenz-1 Displays
881 Presence/Absence Variation and Strong Synteny. Vandepoele K, editor. PLoS ONE. 2016 Oct
882 6;11(10):e0164321.

bioRxiv preprint doi: https://doi.org/10.1101/2021.04.16.440130; this version posted April 16, 2021. The copyright holder for this preprint (which was not certified by peer review) is the author/funder, who has granted bioRxiv a license to display the preprint in perpetuity. It is made available under aCC-BY-NC-ND 4.0 International license.

883 36. Pinosio S, Giacomello S, Faivre-Rampant P, Taylor G, Jorge V, Le Paslier MC, et al. Characterization
884 of the Poplar Pan-Genome by Genome-Wide Identification of Structural Variation. Mol Biol Evol.
885 2016 Oct;33(10):2706–19.
886 37. Redmond SN, Sharma A, Sharakhov I, Tu Z, Sharakhova M, Neafsey DE. Linked-read sequencing
887 identifies abundant microinversions and introgression in the arboviral vector Aedes aegypti. BMC
888 Biol. 2020 Dec;18(1):26.
889 38. Rhoads A, Au KF. PacBio Sequencing and Its Applications. Genomics Proteomics Bioinformatics.
890 2015 Oct;13(5):278–89.
891 39. Lu H, Giordano F, Ning Z. Oxford Nanopore MinION Sequencing and Genome Assembly.
892 Genomics Proteomics Bioinformatics. 2016 Oct;14(5):265–79.
893 40. Mahmoud M, Gobet N, Cruz-Dávalos DI, Mounier N, Dessimoz C, Sedlazeck FJ. Structural variant
894 calling: the long and the short of it. Genome Biology. 2019 Nov 20;20(1):246.
895 41. Huddleston J, Chaisson MJP, Steinberg KM, Warren W, Hoekzema K, Gordon D, et al. Discovery
896 and genotyping of structural variation from long-read haploid genome sequence data. Genome
897 Res. 2017 Jan 5;27(5):677–85.
898 42. De Coster W, D'Hert S, Schultz DT, Cruts M, Van Broeckhoven C, Berger B. NanoPack: visualizing
899 and processing long-read sequencing data. Bioinformatics. 2018 Aug 1;34(15):2666–9.
900 43. Chaisson MJP, Sanders AD, Zhao X, Malhotra A, Porubsky D, Rausch T, et al. Multi-platform
901 discovery of haplotype-resolved structural variation in human genomes. Nature
902 Communications. 2019 Apr 16;10(1):1784.
903 44. Zapata L, Ding J, Willing E-M, Hartwig B, Bezdan D, Jiao W-B, et al. Chromosome-level assembly
904 of *Arabidopsis thaliana* L *er* reveals the extent of translocation and inversion polymorphisms.
905 Proceedings of the National Academy of Sciences. 2016 Jul 12;113(28):E4052–60.
906 45. Michael TP, Jupe F, Bemm F, Motley ST, Sandoval JP, Lanz C, et al. High contiguity Arabidopsis
907 thaliana genome assembly with a single nanopore flow cell. Nature Communications. 2018 Feb
908 7;9(1):541.

bioRxiv preprint doi: https://doi.org/10.1101/2021.04.16.440130; this version posted April 16, 2021. The copyright holder for this preprint (which was not certified by peer review) is the author/funder, who has granted bioRxiv a license to display the preprint in perpetuity. It is made available under aCC-BY-NC-ND 4.0 International license.

909 46. Belser C, Istace B, Denis E, Dubarry M, Baurens F-C, Falentin C, et al. Chromosome-scale
910 assemblies of plant genomes using nanopore long reads and optical maps. Nature Plants. 2018
911 Nov;4(11):879–87.
912 47. Sun S, Zhou Y, Chen J, Shi J, Zhao H, Zhao H, et al. Extensive intraspecific gene order and gene
913 structural variations between Mo17 and other maize genomes. Nat Genet. 2018 Sep;50(9):1289–
914 95.
915 48. Lam ET, Hastie A, Lin C, Ehrlich D, Das SK, Austin MD, et al. Genome mapping on nanochannel
916 arrays for structural variation analysis and sequence assembly. Nat Biotechnol. 2012
917 Aug;30(8):771–6.
918 49. Cao H, Hastie AR, Cao D, Lam ET, Sun Y, Huang H, et al. Rapid detection of structural variation in
919 a human genome using nanochannel-based genome mapping technology. GigaSci. 2014
920 Dec;3(1):34.
921 50. Levy-Sakin M, Pastor S, Mostovoy Y, Li L, Leung AKY, McCaffrey J, et al. Genome maps across 26
922 human populations reveal population-specific patterns of structural variation. Nature
923 Communications. 2019 Mar 4;10(1):1025.
924 51. Leung AK-Y, Liu MC-J, Li L, Lai YY-Y, Chu C, Kwok P-Y, et al. OMMA enables population-scale
925 analysis of complex genomic features and phylogenomic relationships from nanochannel-based
926 optical maps. Gigascience [Internet]. 2019 Jul 1 [cited 2019 Sep 24];8(7). Available from:
927 https://academic.oup.com/gigascience/article/8/7/giz079/5530323
928 52. Soto DC, Shew C, Mastoras M, Schmidt JM, Sahasrabudhe R, Kaya G, et al. Identification of
929 Structural Variation in Chimpanzees Using Optical Mapping and Nanopore Sequencing. Genes
930 (Basel). 2020 Mar 4;11(3).
931 53. Yuan Y, Milec Z, Bayer PE, Vrána J, Doležel J, Edwards D, et al. Large-Scale Structural Variation
932 Detection in Subterranean Clover Subtypes Using Optical Mapping. Front Plant Sci. 2018 Jul
933 17;9:971.

bioRxiv preprint doi: https://doi.org/10.1101/2021.04.16.440130; this version posted April 16, 2021. The copyright holder for this preprint (which was not certified by peer review) is the author/funder, who has granted bioRxiv a license to display the preprint in perpetuity. It is made available under aCC-BY-NC-ND 4.0 International license.

934 54. Dixon JR, Xu J, Dileep V, Zhan Y, Song F, Le VT, et al. Integrative detection and analysis of structural
935 variation in cancer genomes. Nat Genet. 2018 Oct;50(10):1388–98.
936 55. Long E, Evans C, Chaston J, Udall JA. Genomic Structural Variations Within Five Continental
937 Populations of Drosophila melanogaster. G3 (Bethesda). 2018 Aug 15;8(10):3247–53.
938 56. Koren S, Walenz BP, Berlin K, Miller JR, Bergman NH, Phillippy AM. Canu: scalable and accurate
939 long-read assembly via adaptive *k* -mer weighting and repeat separation. Genome Research.
940 2017 May;27(5):722–36.
941 57. Li H. Minimap2: pairwise alignment for nucleotide sequences. Bioinformatics. 2018 Sep
942 15;34(18):3094–100.
943 58. The Arabidopsis Genome Initiative. Analysis of the genome sequence of the flowering plant
944 Arabidopsis thaliana. Nature. 2000 Dec 1;408(6814):796–815.
945 59. Kurtz S, Phillippy A, Delcher AL, Smoot M, Shumway M, Antonescu C, et al. Versatile and open
946 software for comparing large genomes. Genome Biology. 2004;9.
947 60. Jain M, Tyson J, Loose M, Ip C, Eccles D, O'Grady J, et al. MinION Analysis and Reference
948 Consortium: Phase 2 data release and analysis of R9.0 chemistry. F1000Research. 2017 May
949 31;6:760.
950 61. Mi H, Muruganujan A, Ebert D, Huang X, Thomas PD. PANTHER version 14: more genomes, a new
951 PANTHER GO-slim and improvements in enrichment analysis tools. Nucleic Acids Res. 2019 Jan
952 8;47(D1):D419–26.
953 62. Goel M, Sun H, Jiao W-B, Schneeberger K. SyRI: finding genomic rearrangements and local
954 sequence differences from whole-genome assemblies. Genome Biol. 2019 Dec;20(1):277.
955 63. Meyers BC, Kozik A, Griego A, Kuang H, Michelmore RW. Genome-wide analysis of NBS-LRR-
956 encoding genes in Arabidopsis. Plant Cell. 2003 Apr;15(4):809–34.
957 64. Song Y, Ling N, Ma J, Wang J, Zhu C, Raza W, et al. Grafting Resulted in a Distinct Proteomic Profile
958 of Watermelon Root Exudates Relative to the Un-Grafted Watermelon and the Rootstock Plant.
959 J Plant Growth Regul. 2016 Sep 1;35(3):778–91.

bioRxiv preprint doi: https://doi.org/10.1101/2021.04.16.440130; this version posted April 16, 2021. The copyright holder for this preprint (which was not certified by peer review) is the author/funder, who has granted bioRxiv a license to display the preprint in perpetuity. It is made available under aCC-BY-NC-ND 4.0 International license.

960 65. Staal J, Kaliff M, Bohman S, Dixelius C. Transgressive segregation reveals two Arabidopsis TIR-NB-
961 LRR resistance genes effective against Leptosphaeria maculans, causal agent of blackleg disease.
962 Plant J. 2006 Apr;46(2):218–30.
963 66. Li H, Handsaker B, Wysoker A, Fennell T, Ruan J, Homer N, et al. The Sequence Alignment/Map
964 format and SAMtools. Bioinformatics. 2009 Aug 15;25(16):2078–9.
965 67. Krzywinski M, Schein J, Birol I, Connors J, Gascoyne R, Horsman D, et al. Circos: An information
966 aesthetic for comparative genomics. Genome Research. 2009 Sep 1;19(9):1639–45.
967 68. Lin M, Fang J, Hu C, Qi X, Sun S, Chen J, et al. Genome-wide DNA polymorphisms in four Actinidia
968 arguta genotypes based on whole-genome re-sequencing. PLOS ONE. 2020 Apr
969 10;15(4):e0219884.
970 69. Toda N, Rustenholz C, Baud A, Le Paslier M-C, Amselem J, Merdinoglu D, et al.
971 NLGenomeSweeper: A Tool for Genome-Wide NBS-LRR Resistance Gene Identification. Genes
972 (Basel) [Internet]. 2020 Mar 20 [cited 2021 Apr 12];11(3). Available from:
973 https://www.ncbi.nlm.nih.gov/pmc/articles/PMC7141099/

974

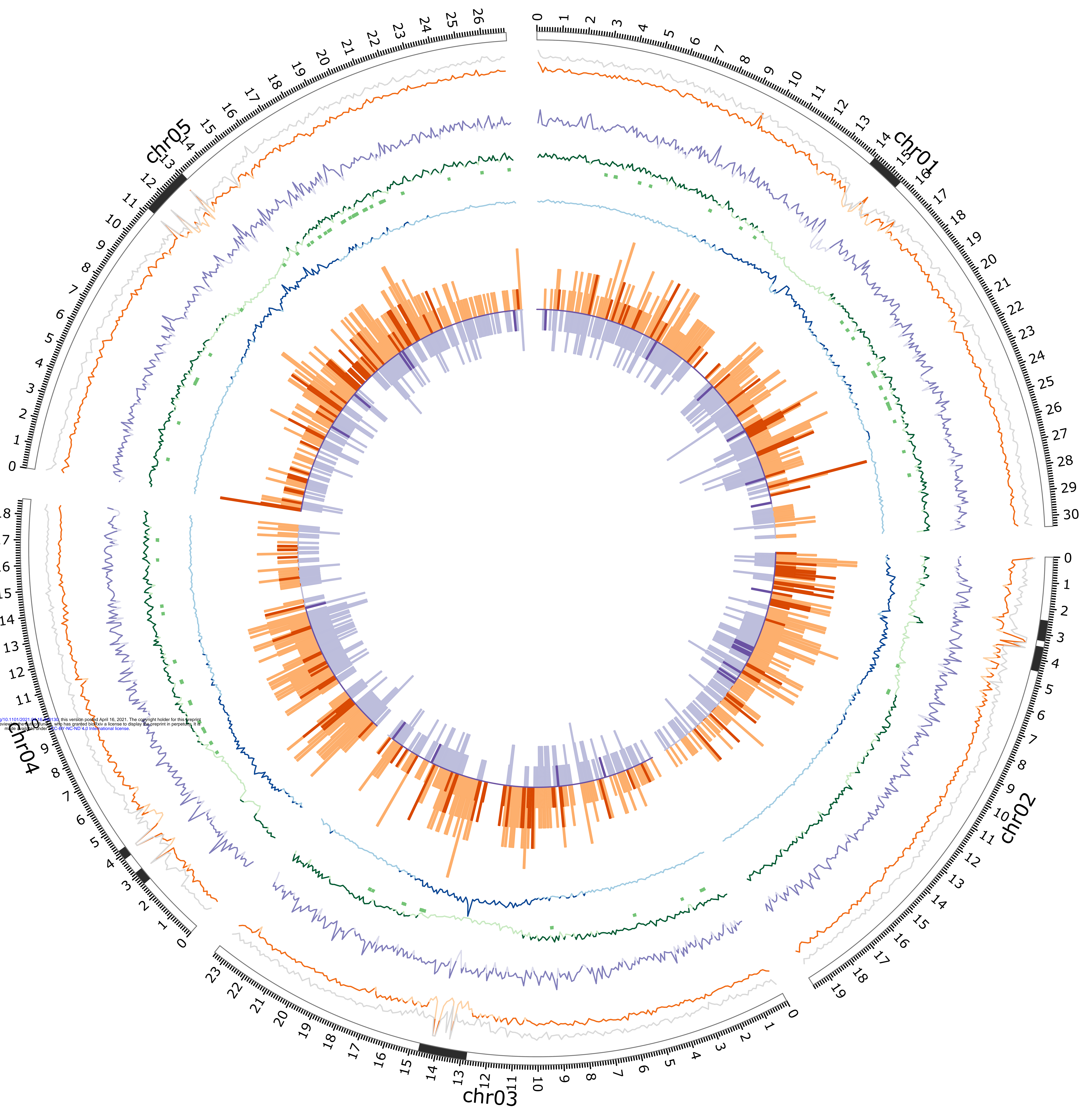

bioRxiv preprint doi: https://doi.org/10.1101/2021.04.16.440130; this version posted April 16, 2021. The copyright holder for this preprint (which was not certified by peer review) is the author/funder, who has granted bioRxiv a license to display the preprint in perpetuity. It is made available under aCC-BY-NC-ND 4.0 International license.